

International Conference on Space Optics—ICSO 2012

Ajaccio, Corse

9–12 October 2012

Edited by Bruno Cugny, Errico Armandillo, and Nikos Karafolas



Efficiency, dispersion and straylight performance tests of immersed gratings for high resolution spectroscopy in the near infrared

J. Fernandez-Saldivar

F. Culfaz

N. Angli

I. Bhatti

et al.



Efficiency, Dispersion and Straylight Performance Tests of Immersed Gratings for High Resolution Spectroscopy in the Near Infra-red

J. Fernandez-Saldivar, F. Culfaz, N. Angli, I. Bhatti,
D. Lobb, G. Baister
Surrey Satellite Technology Ltd., Guildford, UK

B. Touzet, F. Desserouer
Horiba Jobin Yvon SAS, Longjumeau, France

B. Guldemann
European Space Agency, Noordwijk, The Netherlands

Abstract

New immersed grating technology is needed particularly for use in imaging spectrometers that will be used in sensing the atmosphere O₂A spectral band (750nm - 775 nm) at spectral resolution in the order of 0.1 nm whilst ensuring a high efficiency and maintaining low stray light.

In this work, the efficiency, dispersion and stray light performance of an immersed grating are tested and compared to analytical models. The grating consists of an ion-beam etched grating in a fused-silica substrate of 120 mm x 120mm immersed on to a prism of the same material. It is designed to obtain dispersions $> 0.30^\circ/\text{nm}^{-1}$ in air and $>70\%$ efficiency. The optical performance of the immersed grating is modelled and methods to measure its wavefront, efficiency, dispersion and scattered radiance are described. The optical setup allows the measurement of an 80mm beam diameter to derive the bidirectional scatter distribution function (BSDF) from the immersed grating from a minimum angle of 0.1° from the diffracted beam with angular resolution of 0.05° . Different configurations of the setup allow the efficiency and dispersion measurements using a tuneable laser in the 750nm-775nm range. The results from the tests are discussed with the suitability of the immersed gratings in mind for future space based instruments for atmospheric monitoring.

Index Terms— Immersed grating, stray-light, BSDF, grating efficiency, grating dispersion, NIR (*key words*)

I. INTRODUCTION

Immersed grating (IG) technology offers a means to design space borne spectrometers that can achieve improved spectral resolution and spectral quality whilst keeping the size of the spectrometer compact.

Surrey Satellite Technology Ltd. is currently testing the IGs that were designed under ESA contract and manufactured by Horiba Jobin-Yvon (HJY). The gratings were manufactured in a fused silica substrate using ion beam etching techniques and optically contacted onto a prism, of the same material,

manufactured by IC Optical Systems. Both elements were designed to achieve wide spectral dispersion therefore allowing high spectral resolution and at the same time provide high efficiency.

High spectral resolution in Near InfraRed (NIR) is usually required in atmospheric chemistry (or vegetation fluorescence) missions for example in ESA's Sentinel 4 and Sentinel 5 missions. In these missions, the O₂A band (between 750 – 775 nm) is used to derive cloud-top height, aerosols and atmospheric pressure. Accurate measurements of these derived products require fine spectral resolution and high signal-to-noise ratios. This tends to require large system étendue (product of aperture area and solid-angle subtended of the spatial resolution element) to collect sufficient signal in narrow spectral channels with high efficiency.

A demanding specification for measurements in the O₂A band requiring high resolution and high SNR includes spectral dispersion of $>0.24^\circ/\text{nm}$, associated with 70% efficiency with a beam aperture at the grating of at least 80mm in diameter. As an IG is a grating operating in reflection that is illuminated and diffracted in a dielectric medium (with refractive index $\mu > 1$) then the spectral resolution is increased by a factor μ compared to the spectral resolution of the grating in air / vacuum used at the same angles of incidence and diffraction [1].

An illustrative example of an IG designed and tested in this work comprises 1) the grating etched on a fused silica substrate and 2) an immersion prism of the same material is shown in Figure 1.

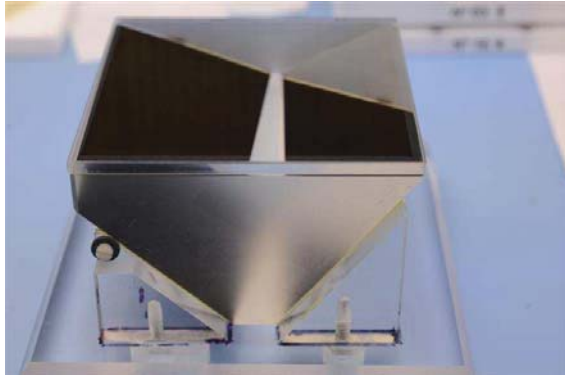


Figure 1: Immersed Grating

In Figure 1, a rectangular substrate with the etched grating is shown at the top of the immersion prism sitting on an acrylic jig used for the optical contacting of both elements. The dimensions of the grating substrate are: 120 mm x 120 mm x 5 mm and the clear aperture where the grating is etched is 110 mm x 110 mm.

The grating shown in Figure 1 was tested in this work to verify its performance according to the models used during its design phase and described in more detail in [1].

II. IMMERSSED GRATING REQUIREMENTS AND DESIGN

The immersed grating under test in this work is immersed in fused silica and it is optimised for the O₂A band. The design of the grating profile is illustrated schematically in Figure 2. This is a trapezoidal model where the grating design parameters are the duty cycle (ratio c/d), the grating period 'd', the groove height and slope angle 'p'.

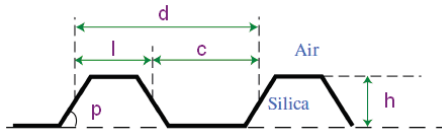


Figure 2: Grating parameters definition

The grating specifications are as follows:

Groove density: $f = 3226 \text{ grooves/mm} \pm 0.2 \text{ grooves/mm}$

Groove height; $h = 450 \text{ nm}$

$c/d = 0.6$

slope = 85°

The grating substrate was then measured using Atomic Force Microscopy (AFM) to determine the geometry of the etched profile. The AFM measurements can only provide an accurate groove height and period determination due to the convolution of the measurement tip with the actual profile. In order to establish the other parameters c/d and p , a model was used in combination of actual measurements of the grating

alone in transmission at a different wavelength and fitted accordingly to derive them.

Five different points of the grating (centre + 4 corners) were measured by AFM. The results shown in Table 1 indicate the average geometry for these points meets with the specification.

Table 1: Grating profile measurements

Sampling point	Measured	Fitted values	
	h	c/d	p (°)
1	458	0.6	83.7
2	496	0.64	85.2
4	493	0.65	85.4
6	498	0.66	85
8	507	0.66	83.4
Average	490	0.64	84.6
Required	450	0.60	85

The grating frequency was also measured directly during AFM measurements and also calculated from the grating equation (described in detail in the section below) for the given geometry and wavelength during interferometric tests.

III. MODEL FOR DISPERSION IN A IMMERSSED GRATING

The basic theory of immersed gratings is well known, and many practical examples have been constructed [2-3]. The basic equation for diffracted beam angles provided by a grating is:

$$\mu_1 \cdot \sin\alpha + \mu_2 \cdot \sin\beta = m \cdot \lambda \cdot f \quad (1)$$

Where,

α is the angle of incidence of light on the grating surface,
 β is the angle of diffraction (on the same side of the normal as the incident beam if α and β are both positive),

m is a positive or negative integer: the diffraction order,

λ is the light wavelength in vacuum,

f is the grating pattern frequency (typically cycles/mm if λ is in mm),

μ_1 is the refractive index of the medium of the incident beam and

μ_2 is the refractive index of the medium of the diffracted beam.

In the case of an IG, both the incident and the diffracted beams are in the same medium, of index μ , so that the equation simplifies to:

$$\sin\alpha + \sin\beta = m \cdot \lambda \cdot f / \mu \quad (2)$$

In principle, light can be diffracted in any order 'm' for which $\sin\beta$ has a real value. In the IG design that is proposed, only the $m = 0$ and $m = 1$ diffraction orders exist (Where $m < 2\mu/\lambda f$). The $m = 0$ order is specular reflection from the grating

surface, which is of interest only as stray light. The usable diffraction is in the first order for which:

$$\sin\alpha + \sin\beta = \lambda \cdot f/\mu \quad (3)$$

The angular dispersion in the immersion medium, produced directly by the grating, is derived by differentiation:

$$d\beta/d\lambda = f/(\mu \cdot \cos\beta) \quad (4)$$

In terms of incident and diffraction angles:

$$d\beta/d\lambda = (\sin\alpha + \sin\beta)/(\lambda \cdot \cos\beta) \quad (5)$$

This formula gives dispersion (radians/nm if λ is in nm) in the medium of index μ . After the diffracted beam emerges from the grating prism into vacuum, the angular dispersion is increased by refraction at the output face. If the light emerges through an exit surface orthogonal to the beam direction, the multiplier is μ , so that dispersion in vacuum is:

$$\text{Dispersion} = \mu \cdot (\sin\alpha + \sin\beta)/(\lambda \cdot \cos\beta) \quad (6)$$

Figure 3 shows the calculated Dispersion in air for 765.5nm incident on the grating at 61.2° for different grating periods (inverse of grating frequency), in red the corresponding Littrow angles (where $\alpha=\beta$) for different grating periods are also shown as a reference.

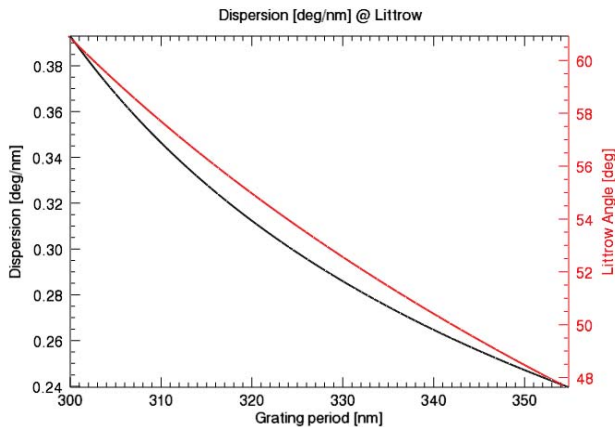


Figure 3: Dispersion model

Figure 4 illustrates the Zemax ray trace model on the IG tested in this work. The red arrows entering the input face of the immersion prism represent the input rays whilst the three rays leaving the prism show the diffracted rays for three different wavelengths. The blue line shows the path of the diffracted ray for 750nm wavelength, the green is for 762.5nm and the red for 775nm.

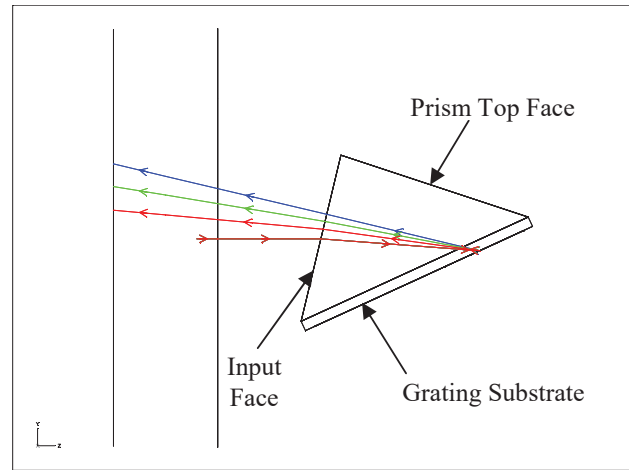


Figure 4: Ray trace in an Immersed Grating

In order to measure the actual dispersion, a laser was tuned in two closely spaced wavelengths λ_1 (762.5 nm) and λ_2 (763 nm). The diffracted beams are then imaged using a CCD camera with a focusing lens where the pixel position of the focused spots is recorded. The angular separation of the focused spots is then calculated from the pixel positions knowing the camera-lens magnification. In order to obtain dispersion, the angular change is divided by the change in wavelength. Preliminary measurements indicate a dispersion of ~ 0.326 °/nm, thus achieving the required specification.

It is important to note that the immersion prism was designed to work near Littrow condition where the angles of incidence and reflection are equal. The exact Littrow condition is used during wavefront measurements (Figure 5), this condition allows the calculation of the grating frequency f from the angles of incidence used knowing the refractive index of fused silica (1.457) for the wavelength used (633 nm).

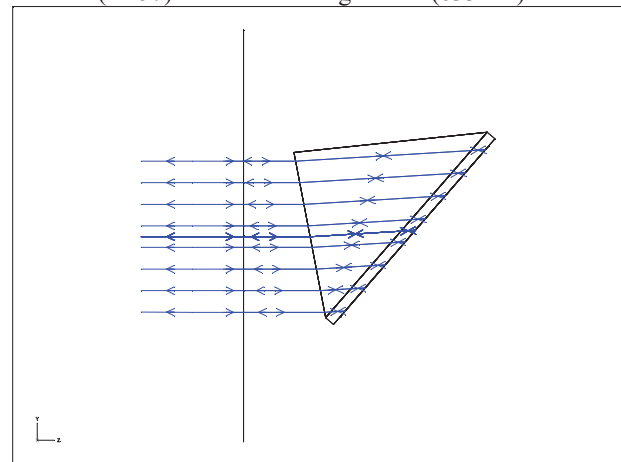


Figure 5: Littrow condition used for interferometric tests

IV. WAVEFRONT

Light will enter and leave the IG through the prism input-output face and the aberration induced is a result of the departure of the surface from flat. When the substrate is optically contacted to the prism it will conform to the prism's contact face so the aberration generated at the prism-substrate interface will be the deviation from flatness of the prism contact face. There will then be an additional aberration generated by the differential flatness of the substrate.

Aberrations will also be produced as a result of non homogeneity in the refractive index of the prism and the substrate. A budget of 0.1λ was placed on the wavefront aberration generated by the non-homogeneity for both components. In calculating the grade of fused silica required to meet the 0.1λ budget it has been assumed that defocus and tilt generated by non homogeneity can be corrected by tilting and defocusing the input beam.

The round trip path length through the prism is estimated at 200mm. In practice the distance travelled through the prism will vary from nearly 0mm at one edge of the aperture to 200mm at the other. An extra tilt term will essentially be introduced as a result of the differences in path length along the aperture but this can be compensated for by tilting the input beam. The absolute refractive index variation required to meet the wavefront budget is $\Delta n = (\Delta W/L) = 0.4 \times 10^{-6}$. This does not account for defocus compensation. Assuming defocus accounts for at least half of the aberration induced by non-homogeneity then material of grade H5 (Maximum Deviation of Refractive Index $\pm 5 \times 10^{-7}$) on the Schott scale is acceptable

The round trip length through the substrate is estimated at 20mm and the required absolute refractive index variation is 3.75×10^{-6} . This variation is acceptable once defocus has been compensated for a material grade of H3 (Maximum Deviation of Refractive Index $\pm 2 \times 10^{-6}$) on the Schott scale. A total budget of 0.25 waves was placed on Horiba Jobin Yvon for the wavefront aberration generated by the manufactured grating.

The total wavefront budget for the IG is detailed in Table 2

Table 2: Wavefront budget

Contributor	Surface/bulk error	Rms wavefront error at 750nm
Input/output surface, 2 passes	0.5 fringe rms (633nm)	0.2
Bulk inhomogeneity, 20cm path	0.1 waves rms	0.1
Prism contact face	0.25 fringe rms (633nm)	0.2
Substrate differential flatness	0.25 fringe rms (633nm)	0.2
Grating phase errors	0.25 period rms	0.25
Total wavefront aberration, rms waves		0.45

Wavefront aberration was measured using a Fisba μ -Phase2 1000 phase-shifting Twyman-Green Interferometer from Trioptics. A μ Lens Plano 100 lens objective was used as it allows a sample diameter of up to 101.6mm. The configuration

used for the IG wavefront measurement requires Littrow condition as shown in Figure 5.

The IG wavefront setup was calibrated using an optical flat prior to measurements with the IG. The results of the IG wavefront is depicted in Figure 6 and do not include any masking of the clear aperture of the IG.

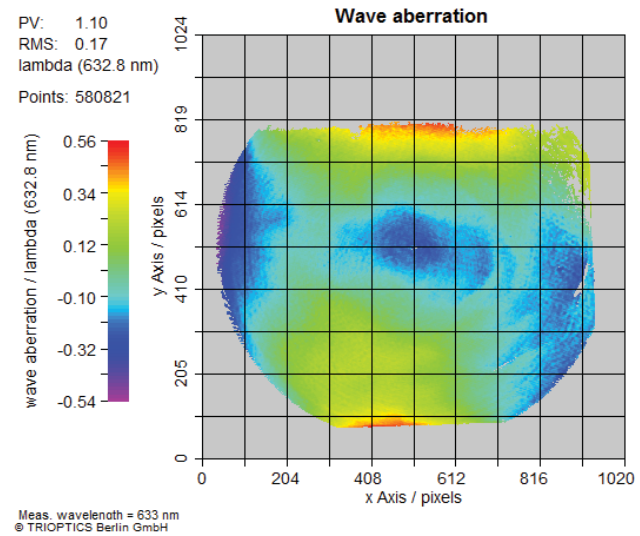


Figure 6: Wavefront Image of Immersed Grating

The IG Root Mean Square (RMS) wavefront variation measured was 0.17λ @ 632.8nm we can infer from this that the wavefront error at the shortest wavelength to be used (750nm) meets the wavefront budget specification.

V. GRATING EFFICIENCY AND POLARISATION

During the grating design phase, efficiency was calculated for TE, TM and unpolarised light assuming a rectangular grating profile. The calculated efficiency curves for both polarisations are shown in Figure 7.

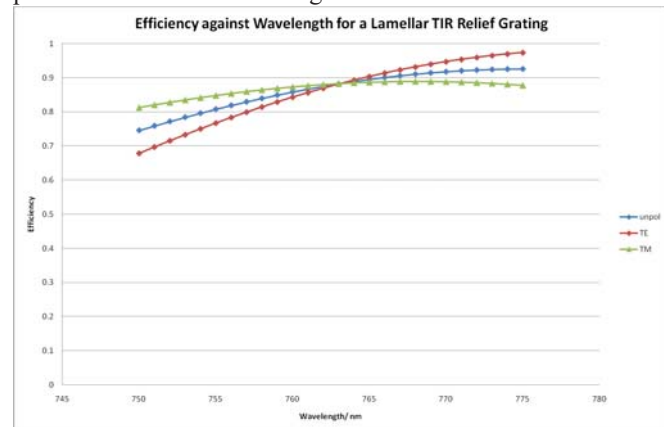


Figure 7: Immersed Grating theoretical efficiencies

Horiba Jobin Yvon optimised the grating performance in profile shapes for low polarization dependence. Grating

efficiency calculations were performed by HJY after AFM measurements taking into account the actual shape of the profile on the final gratings. HJY developed a cross measuring method based on efficiency measurement using UV-VIS light and then using theoretical efficiency calculation fitting. The calculated efficiencies by HJY on five sampling points are shown in Table 3 below.

Table 3: IG Calculated Efficiency

Sampling point	Calculated Efficiency			
	1T TE	1T TM	0T TE	0T TM
1	0.928	0.409	0.051	0.572
2	0.971	0.405	0.008	0.574
3	0.968	0.365	0.011	0.613
4	0.968	0.351	0.012	0.628
5	0.965	0.349	0.02	0.634
Average	96.00%	37.58%	2.04%	60.42%

The measurements by HJY on the same five sampling points are shown in Table 4 below.

Table 4: IG Measured Efficiency

Sampling point	Measured Efficiency			
	1T TE	1T TM	0T TE	0T TM
1	0.937	0.408	0.048	0.568
2	0.960	0.394	0.008	0.563
3	0.968	0.360	0.011	0.608
4	0.971	0.348	0.013	0.624
5	0.968	0.345	0.020	0.632
Average	96.08%	37.10%	2.00%	59.90%

Once the efficiency has been calculated for a point at a single wavelength, this can be extrapolated according the efficiency model for the given geometry, this is seen in Figure 8 for the unpolarised case.

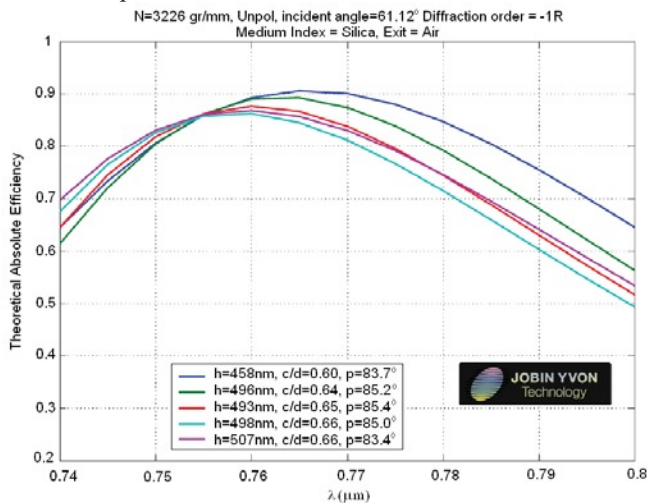


Figure 8: Theoretical Absolute Efficiencies from AFM measurements

Efficiency peaks in the wavelength of interest 750nm - 775nm.

VI. STRAYLIGHT MEASUREMENTS SETUP

The optical setup to determine the stray light from the IG is depicted in Figure 9.

- Light from a Toptica DL100 tunable diode laser is coupled into a single mode fibre. The wavelength range is 750-775nm.
- The beam from the fibre is projected on a square aperture that allows spatial scanning of the IG as this can be moved with respect to the beam to cover the entire area of the IG.
- The output from the fibre is reimaged and filtered onto the front focal plane of a spherical mirror (500mm focal length, 190mm diameter) with surface roughness specified to 0.5nm RMS (A prism acts as a fold mirror and provides aberration correction as the spherical mirror is used off axis).
- The spherical mirror collimates the filtered laser light producing a collimated beam (40mm x 40mm) as an input to the IG near the Littrow angle.
- The IG diffracts the collimated beam, it is mounted on a rotation stage, tilt platform and XYZ stage that allows spatial scanning of different areas on the IG.
- The diffracted beam is re-imaged by the same spherical mirror onto the Stray Light Plane (SLP).
- At the SLP the main diffracted spot is physically blocked by means of a cross-hair using two crossed pins, each having a width of 0.87mm.
- The stray light focal plane is re-imaged onto a CCD-based camera with imaging lens (Nikkor 85mm F1.4) combined with a 200mm focal length close up achromat lens.

Depending on the wavelength chosen at the laser monitored with a precision wavelength meter (High Finesse WS5) a focused spot will be formed in the stray light plane. Any stray light generated by the grating will leave the immersed prism at a different angle than the originally diffracted beam and therefore will also appear at the stray light plane around the focused spot. The system allows stray light to be collected over a field 12° square. Any scattered light produced by all the elements in the setup can be calibrated by inserting a super-polished mirror with surface roughness in the ~5Å in place of the immersed prism. This mirror is considered perfect and it is used to isolate the stray light contributions from the immersed prism.

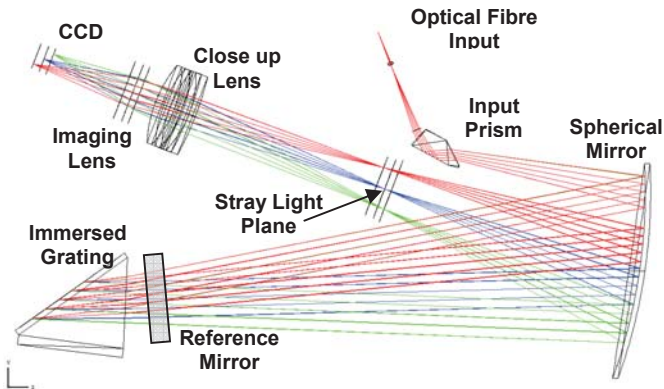


Figure 9: Test setup for stray light measurements

The design of the setup allows stray light distribution to be captured within $\pm 6^\circ$ from the diffracted spot at order -1 with an angular equivalent resolution of approximately 0.05° .

The setup built to test straylight, dispersion and efficiency of the complete IG is shown in Figure 10 below.



Figure 10: Test setup

Zemax was used to simulate experimental setup described in Figure 9. From this, the two-dimensional scatter distribution was calculated including the blocking by the cross hair in an area corresponding to $\pm 6^\circ$. This is shown in Figure 11.

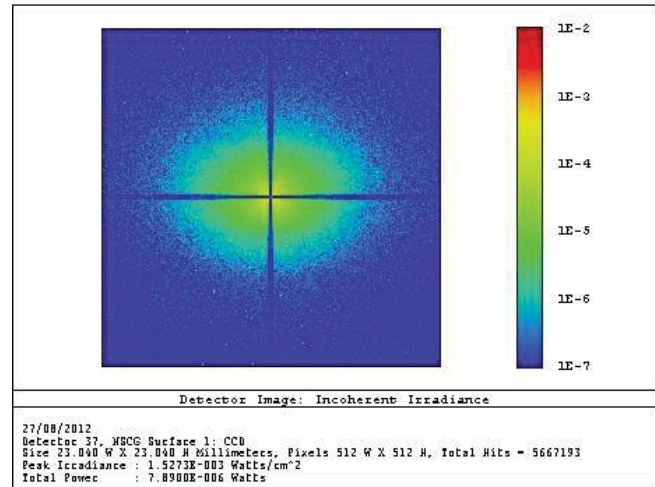


Figure 11: Calculated irradiance at SLP

This scattered distribution analysis does not account for diffraction which can be calculated separately for the geometry of the test setup using Zemax Non-Sequential model.

Given the square shape of the collimated beam onto the IG, a cross-shaped diffraction pattern is expected at the stray light plane. Zemax diffraction calculation is shown in Figure 12.

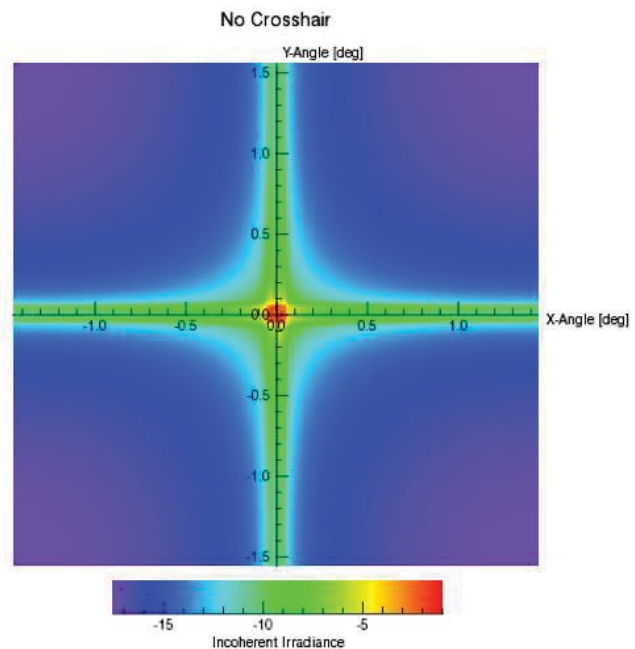


Figure 12: Relative Incoherent Irradiance at SLP with Diffraction

There is a minimum angle where the scattered distribution can be considered dominant over diffraction effects. This angle is $\sim 0.1^\circ$ from orthogonal axis from the focused spot. At this angle, the irradiance due to diffraction is more than 8 orders of magnitude smaller than in the main focused spot.

In practice, measurements in this region $<0.1^\circ$ are physically blocked by the cross-hair at the SLP.

The cross-hair is positioned with respect to the input wavelength according to the position of the diffracted spot. Figure 13 shows 3 different images of the diffracted spot from the IG at three different wavelengths (775nm, 762.5nm and 750nm respectively)

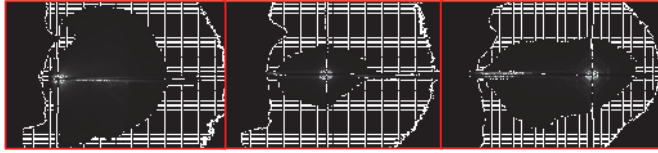


Figure 13: Diffracted spot positions with cross-hair in place for the wavelengths (775, 762.5 and 750nm respectively).

It is important to note that the crosshair is blocking the focused spot, what is observed around the centre of the cross-hair is the scattered distribution around the spot. In addition, horizontal diffraction 'streaks' are observed away from the centre of the spot that are not blocked by the crosshair. The software developed using Matlab allows the masking of these areas. Figure 14 shows an experimentally obtained image, imported into Matlab, of the super-polished mirror blocked by the two orthogonal pins. The mirror is used as a reference that is put in the same position as the IG and is angled to direct the reflected beam so that it is focused in the same position as the diffracted beam from the IG.

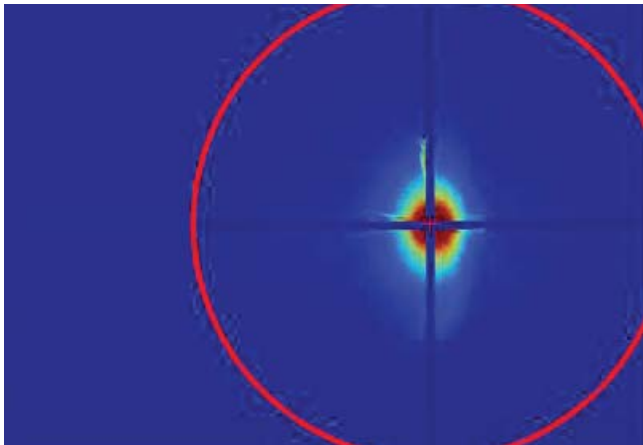


Figure 14: Normalised power measurement

The red circle represents the maximum angle considered for BSAF calculations $\sim 6^\circ$. The physical crosshair covers the central diffraction beams generated by the square aperture. This crosshair is also masked during analysis for BSAF.

A closer look comparing the spots generated at SLP by the reference mirror and the IG reveals a ring-like structure around the diffracted spot (Figure 15). Possible causes for the ring structures might be related to the specific production of this grating.

In Figure 15, the image of the mirror (left) and IG (right) is shown at the stray light plane.

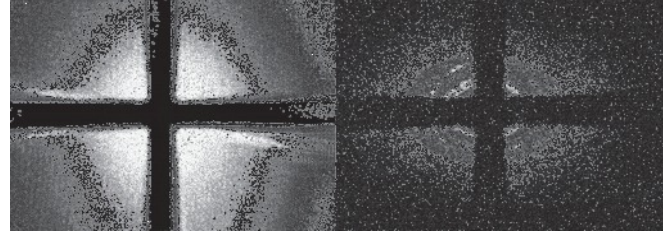


Figure 15: Mirror and Immersed Grating

The intensity of the brightest ring (innermost) is ~ 3 orders of magnitude smaller than the intensity on the focused spot revealed when the cross-hair pins are removed and the integration time is adjusted accordingly.

VII. BI-DIRECTIONAL SCATTER DISTRIBUTION FUNCTION (BSDF)

The bidirectional scatter distribution function, BSDF, is used to describe the scatter distribution for the IG. The model's geometry is shown in Figure 16.

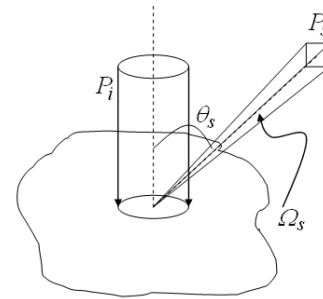


Figure 16: BSAF model

$$BSDF = \frac{P_s / \Omega_s}{P_i \cos \theta_s} = \frac{A}{B + \theta_s^g} \quad (6)$$

From Equation 6 it can be seen that the scattered light for a given angle can also be analysed using an ABg scattering model which is a commonly used method for defining the BSDF. It is generally a good model to use when the scattering is mainly due to random isotropic surface roughness, and the scale of the roughness is small compared to wavelength of light being scattered. These assumptions are generally valid for polished optical surfaces, so it is applicable to the IG.

The BSDF has been determined experimentally using the setup described in section VI. Since the scatter distribution is a function of angle and given rotational symmetry of the spots it is possible to obtain a radial average of the distribution the angles. This is shown for the measurements obtained with the IG (red line) and super polished mirror (blue line) in Figure 17.

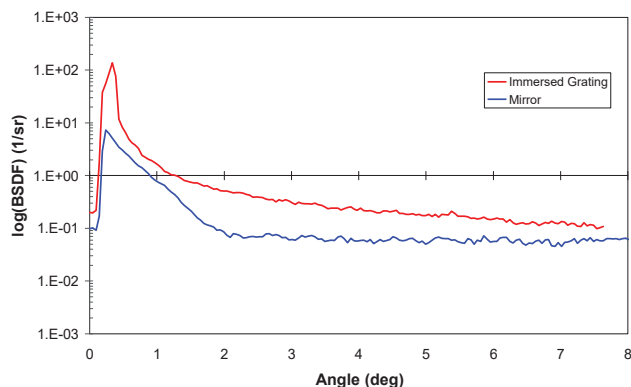


Figure 17: Mirror and Immersed Grating

The figure above indicates that the mirror can be used as a reference to derive the BSDF of the IG with higher scattering characteristics. It is important to note that at a certain angle the distributions appear to flatten, this is observed more in the mirror due to the low scattering but this is an effect of the high dynamic range, explained in more detail below.

Given the high dynamic range nature of the BSDF compared to the limited dynamic range (DR) of the CCD, it is only possible to extend the captured dynamic range by means of neutral density filters or multiple exposures of different integration time that allow a continuous measurement from very high to very low intensity values. Figure 18 illustrates the approach of multiple exposures with a factor that effectively reduces the signal level to a known amount. This allows the extended DR, in this case by means of a Neutral Density filter. This can be seen in Figure 18 where an image with a longer exposure was captured; this allows BSDF measurements at greater angles from the main spot.

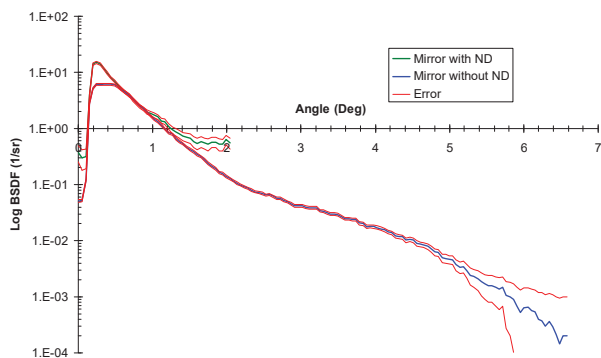


Figure 18: Extending Dynamic Range

By means of multiple exposures it is possible to obtain a good SNR (50:1) for angles $\pm 6^\circ$. The calculated signal to noise obtained for each radial bin of 0.05° is shown in Figure 19 and it demonstrates that measurements at longer angles are possible in spite of the low scattering expected.

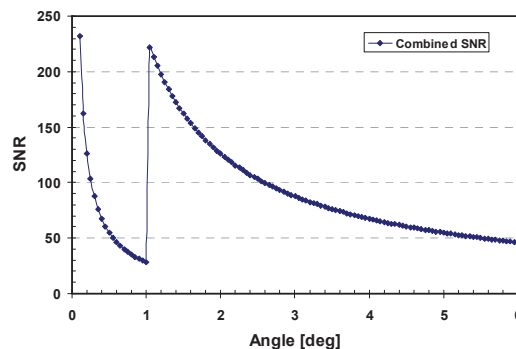


Figure 19: Signal to Noise

Once all the measurements are completed for the wavelengths of consideration, it will be possible to fit the data to an ABg scattering model of the IG and calculate estimates of the Total Integrated Scatter (TIS). The characterisation of the IG straylight performance it is important for future instruments based on this technology.

CONCLUSIONS

An IG in near Littrow configuration was tested for stray light performance. Dispersion $> 0.30/\text{nm}^{-1}$ in air and $>70\%$ efficiency was achieved. The optical performance of the IG was modelled analytically using Zemax ray tracing software. The methods to determine the diffracted wavefront, grating efficiency, dispersion and scattered radiance of the immersion grating have been described. BSDF has been determined from the setup, from a minimum angle of 0.1° from the diffracted beam with angular resolution of 0.05° . Different configurations of the setup enabled the efficiency and dispersion measurements to be measured using a tunable diode laser in the 750nm-775nm wavelength range

The IG is now ready for thermal cycling trials, with any change in performance due to the test campaign being evident after subsequent tests and comparisons to the same mirror reference. The results from these tests should enable determining the suitability of the IGs to be used for future space based instruments for atmospheric monitoring.

ACKNOWLEDGEMENT

The NIR-IG development is being performed by Surrey Satellite Technology Ltd. (SSTL) under ESA contract Contract No. 4200023122/10/NL/RA. The fused silica gratings are being developed by Horiba Jobin Yvon under contract to SSTL. The authors would like to thank Dr. Chris Pietraszewski and Terry Dines from IC Optical Systems for the optical contacting of the IG under test. The SSTL authors would also like to thank James Pursehouse for his valuable contribution to the analysis shown in this paper.

REFERENCES

- [1] [1] J. Fernandez-Saldivar; I. Bhatti; D. Lobb; B. Touzet; B. Guldimann, "Straylight measurements of immersed gratings for high-resolution spectroscopy in the near

- infrared”, SPIE Optical Design and Engineering IV, Jean-Luc M. Tissot; Laurent Mazuray; Jeffrey M. Raynor; Rolf Wartmann; Andrew Wood, Editors. October 2011.
- [2] Szumski and Walker, “The Immersed Echelle - Basic Properties”, Mon. Not. R. Astron. Soc. 302, 139-144 (1999).
- [3] Marcianite, Hirsh, Raguin and Prince, J., “Polarization-Insensitive High-Dispersion Total Internal Reflection Diffraction Gratings”, J. Opt. Soc. Am. A Vol. 22, No. 2, (2005).